Two-body fragmentation dynamics of $C_2H_2^{2+}$ by electron impact: Disentangling vinylidene decarbonation from symmetric breakup

Lei Chen,[1] Xu Shan,[1] Enliang Wang,[2] Xueguang Ren,[2,3] Xi Zhao,[1] Weizhe Huang,[1] and Xiangjun Chen[1,*]

[1]*Hefei National Laboratory for Physical Sciences at the Microscale and Department of Modern Physics, University of Science and Technology of China, Hefei 230026, China*

[2]*Max Plank Institute for Nuclear Physics, Heidelberg 69117, Germany*

[3]*School of Science, Xi'an Jiaotong University, Xi'an 710049, China*

(Received 4 September 2019; published 16 December 2019)

We report experimental investigations of two-body fragmentation of $C_2H_2^{2+}$ induced by 1 keV electron collision utilizing an ion momentum imaging spectrometer. With the ion-ion coincidence measurement, dissociation channels $C_2H_2^{2+} \rightarrow H^+ + C_2H^+$ (deprotonation) and $C_2H_2^{2+} \rightarrow H_2^+ + C_2^+$ (H_2^+ formation) are directly identified, while the symmetric breakup $C_2H_2^{2+} \rightarrow CH^+ + CH^+$ channel and vinylidene decarbonation $C_2H_2^{2+} \rightarrow C^+ + CH_2^+$ channel are not well separated in the measured time-of-flight (TOF) correlation map. In this work, by taking advantage of the independence of kinetic energy release (KER) on the dissociation angle, we are able to disentangle the events from the TOF map. Consequently, KER distributions for all four fragmentation channels are deduced, and the relative branching ratios are precisely determined from the measurements. By comparing the measured KER values with the previous calculated potential energy surfaces, pathways for the fragmentation channels are assigned.

DOI: 10.1103/PhysRevA.100.062707

I. INTRODUCTION

The existence of molecular dications in the gas phase has attracted considerable attention in physics, chemistry, as well as biology because it challenges the fundamentals of chemical bonding and plays important roles in a wide range of sciences and technologies, such as radiation damage, interstellar chemistry, and the plasma industry. For one example, the bond-forming reactions of hydrocarbon dication provide a possible route for the formation of larger polycyclic aromatic hydrocarbons in interstellar environments [1]. Electrons in molecules can be removed by interactions with energetic photons, highly charged ions, and electrons as well as intense laser field, among which electrons are important radiation sources in an interstellar medium, planetary atmosphere, and plasma etching processes. Driven by the Coulomb repulsive forces between the charged centers, the unstable ionized molecules will dissociate into fragments. One of the key tasks in this field is to figure out which parameters control the fragmentation pathway. In the past several decades, great progress has been made in the development of multiple coincidence ion momentum imaging techniques [2,3], making it feasible to reveal multibody fragmentation dynamics for small molecules.

Acetylene (C_2H_2) is one of the simplest stable hydrocarbons widely existing in the planetary atmosphere and interstellar medium. In recent years, acetylene dication ($C_2H_2^{2+}$) has been extensively studied both theoretically [4–10] and experimentally as a prototype for investigating superfast deprotonation [11], proton migration (molecular isomerization) [12–19], and H_2^+ formation [20–22]. Various techniques were applied to investigate fragmentation of $C_2H_2^{2+}$, and four possible two-body dissociation channels were observed, i.e., (i) deprotonation channel $H^+ + C_2H^+$, (ii) H_2^+ formation channel $H_2^+ + C_2^+$, (iii) acetylene symmetric breakup channel $CH^+ + CH^+$, and (iv) vinylidene decarbonation channel $C^+ + CH_2^+$. Among these channels, channel $C^+ + CH_2^+$ has attracted intensive attention [12–19,23–25] because of the embedded isomerization process from acetylene dication $[HCCH]^{2+}$ to vinylidene dication $[HHCC]^{2+}$. Experiments performed by extreme ultraviolet [23,25] and an intense laser field [12,24] have revealed that the isomerization process can occur through the $A\,^2\Sigma_g^+$ state of $[HCCH]^+$ by absorbing photons in two steps on a time scale of about 50 fs, or through the $1\,^3\Pi$ state of $[HCCH]^{2+}$ by absorbing multiple photons in one step.

It is worthwhile to note that channel $CH^+ + CH^+$ and channel $C^+ + CH_2^+$ are too close on the time-of-flight (TOF) correlation map to be clearly separated by the momentum conservation condition, especially in the case of low extraction electric field [16,26,27]. This problem can be partially solved by increasing the strength of the field, as was done in Refs. [4,17,23,24,28–32]. However, a higher extraction electric field may decrease the momentum resolution of the spectrometer. This is a common feature in the investigations of the fragmentation of hydrocarbons having multiple hydrogen atoms. Since the mass of the hydrogen atom is very low, the deprotonated and protonated channels overlap strongly in the TOF correlation map. Deuteration is an alternative way [15,19,33–36] to better separate the explored channels, which, however, requires highly demanding target molecules. Therefore, a general method is needed to disentangle fragmentation channels of charged hydrocarbons with small differences in the mass of the fragments.

*xjun@ustc.edu.cn

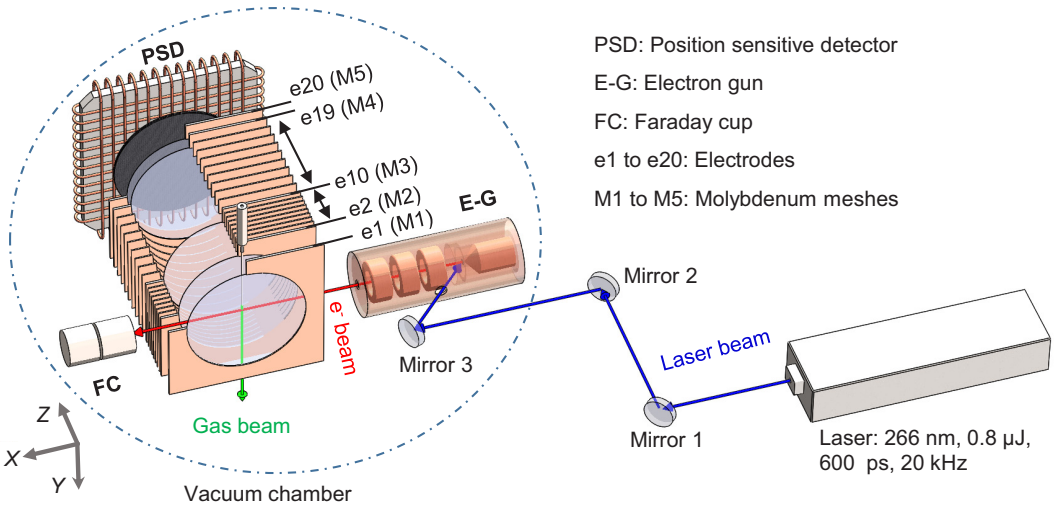

FIG. 1. Schematic diagram of the experimental setup.

Additionally, we notice that investigations of the dissociation of $C_2H_2^{2+}$ by electron impact are still scarce. King *et al.* [30] observed channels $H^+ + C_2H^+$, $CH^+ + CH^+$, and $C^+ + CH_2^+$ from their ion pair coincidence TOF maps by electron impact at energy from 35 to 200 eV. They obtained branching ratios for charge-separating dissociation of $C_2H_2^{2+}$ at various impact energies, and they deduced kinetic energy release (KER) values for channels $H^+ + C_2H^+$ and $CH^+ + CH^+$ with the help of Monte Carlo (MC) simulations. Flammini *et al.* [18,37] observed channels $H^+ + C_2H^+$ and $C^+ + CH_2^+$ in their Auger-electron-ion-ion coincidence map measured by electron impact at 4 keV, and they extracted the corresponding KER values from the map. They concluded that the isomerization process selected by the Auger electron is prior to occurring in the ground state and the low-lying excited states of $C_2H_2^{2+}$. Very recently, Luo *et al.* [26] reported their investigation on channel $CH^+ + CH^+$ and channel $C^+ + CH_2^+$ by cold target recoil-ion momentum spectroscopy at an electron impact energy of 100 eV. KER distribution for channel $CH^+ + CH^+$ was deduced by MC simulation, although channel $C^+ + CH_2^+$ cannot be separated from channel $CH^+ + CH^+$ under the weak extraction field condition (∼24 V/cm).

In this work, the two-body fragmentation of $C_2H_2^{2+}$ is studied experimentally using a newly built ion momentum imaging spectrometer. The precursor $C_2H_2^{2+}$ is created by the collision of an effusive acetylene molecular beam with 1 keV electrons emitted from a photoelectron emission gun. By measuring the TOF correlation map, the $H^+ + C_2H^+$ and $H_2^+ + C_2^+$ channels can be identified, while the events of channel $C^+ + CH_2^+$ are overlapped with those of channel $CH^+ + CH^+$. A method that is based on the fact that KER is independent of the dissociation angle has been developed to disentangle the events of the latter two channels from the mixture. KER distributions, as well as relative branching ratios for these channels, are precisely obtained. With the aid of the potential energy surfaces (PESs) and theoretical calculations in the literature, we are able to elucidate fragmentation pathways of four channels observed in the present work.

II. EXPERIMENTAL METHODS

The experiment is performed using an ion momentum imaging spectrometer recently built in our laboratory. As shown in Fig. 1, a pulsed electron beam from a photoelectron emission gun collides with the gas target in the reaction zone. Details on the working principle of the photoelectron emission gun can be found in Ref. [38]. Briefly, electron pulses are emitted from a tantalum cathode that is illuminated by a 266 nm pulsed laser. The pulsed electron beam is then accelerated and focused to generate a parallel electron beam. The repetition rate and pulse duration of the laser are 20 kHz and 0.6 ns. The optic mirrors 1 and 2 are used to collimate the laser beam, while mirror 3 is mounted on the electron gun in the vacuum chamber to reflect the laser beam onto the cathode. The uncollided electron beam is dumped by a set of Faraday cups, which include a 1-mm-diam inner cup and a 6-mm-diam outer cup. The electron beam currents collected by the inner and outer cups are monitored by two picoammeters (Keithley Model 6485). The total average electron beam current of 60 pA can be obtained during the experiments. The spot size of the electron beam is collimated to about 1 mm diam at the reaction zone. An effusive gas target is introduced to the reaction zone by a copper capillary mounted on a three-dimensional manipulator. The internal diameter and length of the capillary are 0.1 and 60 mm, respectively. The target particle density in the reaction zone is estimated to be about $10^{12}/cm^3$.

After the collision of electrons with the molecular target, the fragment ions are analyzed by a Wiley-Mclaren type time-of-flight mass spectrometer (TOF-MS) [39] followed by a two-dimensional (2D) time- and position-sensitive detector (PSD). The TOF-MS comprises 20 oxygen-free copper plane electrodes (e1–e20) and five molybdenum meshes (M1–M5). The three-dimensional size of the electrode e3–e9 and e11–e18 is 120 mm × 120 mm × 1 mm, while that of e1, e2, e10, e19, and e20 is 120 mm × 120 mm × 2 mm. All the electrodes have a 100-mm-diam center hole. TOF-MS consists of three parts: an extraction region (e1–e2), an acceleration region (e2–e10), and a drift region (e10–e20). A pair of pulsed

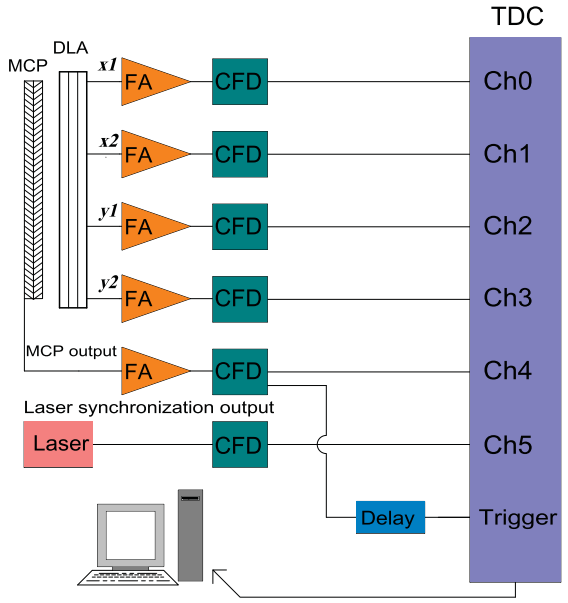

FIG. 2. Schematic diagram of the data acquisition system. MCP: microchannel plate, DLA: delay line anode, FA: fast amplifier, CFD: constant fraction discriminator, TDC: time to digital converter.

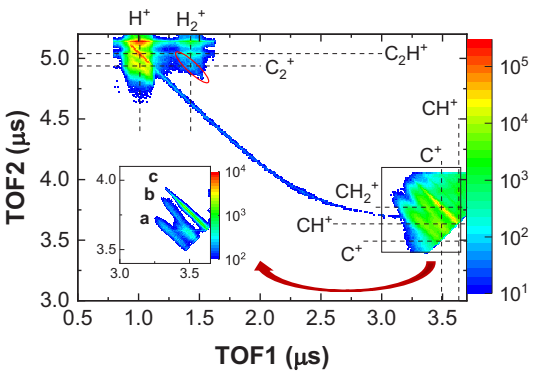

FIG. 3. TOF correlation map of ionic fragments created in collisions of 1 keV electrons with C_2H_2. TOF1 and TOF2 are TOFs of the first hit ion and second hit ion. The inset is the enlarged image of C-C bond breaking channels. Coincidence islands in the inset are as follows: *a*, channel $C^+ + C^+$ (+ 2H); *b*, channel $C^+ + CH^+$(+H); *c*, channel $CH^+ + CH^+/C^+ + CH_2{}^+$.

voltages with opposite polarities (DEI PVM-4210) is applied to M1 and M2 to generate a pulsed electric field to extract the fragment ions into the acceleration region. The transmission rate of each mesh for M1–M4 is 81%, while that of M5 is 64%. A voltage-divider using a resistor chain ($8\times R$, $R = 1\,\mathrm{M\Omega}$, with 0.1% tolerance) is employed to maintain the uniform electric field in the acceleration region. The lengths of the extraction and acceleration regions are 20 and 40 mm, respectively, while the length of the drift region is 100 mm. The PSD consists of a pair of microchannel plates (MCPs) of 100 mm diam in a chevron configuration and a delay line anode (DLA) [40,41].

The schematic diagram of the data acquisition system is shown in Fig. 2. The MCP output signal and four decoupled DLA signals (*x1*, *x2*, *y1*, *y2*) are first amplified by five fast amplifiers with a gain of 150, and then these five signals together with the laser synchronization signal are discriminated by constant fraction discriminators (CFD, ORTEC 935). The discriminated MCP signal will be delayed 12 μs to trigger a multihit time to digital converter (TDC, CAEN 1290N). The TDC has a time resolution of 25 ps and a 52 μs measuring range. The digitized data from TDC are stored event by event on a computer disk for off-line data analysis. The TOF of each ion can be deduced by the difference between its MCP output signal and the laser synchronization signal with a fixed time delay. The position of each ion hit on the detector can be obtained with four DLA output signals. The three-dimensional momentum of the ion is reconstructed from its TOF t and position (x, y),

$$p_x = m\frac{x}{t}, \tag{1}$$

$$p_y = m\frac{y}{t}, \tag{2}$$

$$p_z = qE(t_0 - t), \tag{3}$$

where $p_i (i = x, y, z)$ are the momentum components of the detected ion at the moment of fragmentation. m and q represent the mass and charge of the ion. E is the strength of the extraction field. t_0 is the central value of the TOF corresponding to the ions with zero momentum along the extraction axis (z-axis). It is worthwhile to mention that Eq. (3) is an approximation that is valid only when the initial kinetic energy of the ion in present experiment is much smaller than that obtained in the extraction and acceleration region, which is the case in the present work. The kinetic energy of the ion can thus be deduced.

A stainless steel (316L) spherical vacuum chamber of diameter 450 mm is used to house the spectrometer. The chamber is pumped by a 700 l/s turbo-pump (Pfeiffer Hipace700) backed by an oil-free scroll vacuum pump (Anest Iwata ISP-250C). The background pressure in the chamber is better than 1×10^{-6} Pa after bakeout.

In this work, the impact energy of the electron beam is 1 keV and the average beam current is about 40 pA. A multicoincidence method [42] is used to improve the detection efficiency of ion pairs, that is, only the events with at least two fragment ions will be recorded. The electric fields in both the extraction and the acceleration region are 50 V/cm. With the sample gas loaded, the working pressure in the reaction chamber is maintained at about 4×10^{-5} Pa.

III. RESULTS AND DISCUSSION

A. Identification of two-body fragmentation channels

The TOF correlation map of C_2H_2 ionic fragments is shown in Fig. 3. For a certain dissociative channel, the true events will distribute along an island on the map due to the momentum correlation. Six correlation islands are identified in Fig. 3. For channel $C_2H_2{}^{2+} \rightarrow H^+ + C_2H^+$, a shape island accompanied by a long tail can be clearly observed. A detailed investigation has revealed that this long tail originates from a long-lived metastable dication with a mean lifetime of 1695 $\pm$ 144 ns [43]. Close to the main feature of channel $H^+ + C_2H^+$, channel $H^+ + C_2{}^+$(+H) and channel $H_2{}^+ + C_2{}^+$ are

TABLE I. KER values for two-body fragmentation channels of $C_2H_2^{2+}$.

	KER (eV)							
	Electron impacts			Intense laser	Photoionization		Ion collisions	
Channel	Present	4 keV[a]	30–200 eV[b]	790 nm[c]	42 eV[d]	31.9–50 eV[e]	200 keV He^{2+} ion[f]	3 keV/u Ar^{8+} ion[g]
$H^+ + C_2H^+$	3.6	6.47	3.5 ± 0.5[h]	~3.7	3.75	~4.4		4.6
	4.8			~4.9	4.75			
$H_2^+ + C_2^+$	4.4						4.45	
$CH^+ + CH^+$	5.0			~4.8	5.0	~5.2		5.0
	~6.0			~6.2		~7.7		
	~8.0							
$C^+ + CH_2^+$	4.5	5.9 ± 2.7	3.5 ± 0.5[i]	~4.4	4.5	~4.4		4.5
	5–7							6.0

[a]References [18,37].
[b]Reference [30].
[c]Reference [44].
[d]Reference [6].
[e]Reference [28].
[f]Reference [20].
[g]Reference [31].
[h]At 55 eV electron energy.
[i]At 65 eV electron energy.

recognized. On the bottom right corner of Fig. 3, which is enlarged in the inset, fragmentation channels *a*: $C^+ + C^+$ (+2H) and *b*: $C^+ + CH^+$(+H) can also be observed, while island *c* is a mixture of the events of channel $C^+ + CH_2^+$ and channel $CH^+ + CH^+$, which cannot be distinguished from each other in the TOF correlation map. This dilemma has also been encountered in previous works [16,17,26,27]. One possible solution is to increase the extraction electric field imposed on the TOF spectrometer [4,17,23,24,28–32]. Here an alternative analysis method is introduced to disentangle these two channels with almost no limitation on the strength of the electric field. Therefore, in this work, four two-body fragmentation channels of $C_2H_2^{2+}$ will be analyzed and discussed:

$$C_2H_2^{2+} \rightarrow H^+ + C_2H^+, \quad (4)$$

$$C_2H_2^{2+} \rightarrow H_2^+ + C_2^+, \quad (5)$$

$$C_2H_2^{2+} \rightarrow CH^+ + CH^+, \quad (6)$$

$$C_2H_2^{2+} \rightarrow C^+ + CH_2^+. \quad (7)$$

Total KER distributions as well as branching ratios for these four channels are obtained. The results are presented in Tables I and II, together with some previous results in the literature for comparison.

B. Deprotonation channel $H^+ + C_2H^+$

Deprotonation channel $H^+ + C_2H^+$ was observed by Flammini *et al.* [37] in their Auger-electron-ion-ion coincidence experiment by electron impact at 4 keV. The average kinetic energy of the fragments C_2H^+ and H^+ was estimated to be 0.25 and 6.22 eV from the TOF. King *et al.* [30] were able to distinguish this channel from ion pair coincidence TOF measurement. With the help of MC simulation, a single KER value of 3.5 ± 0.5 eV was determined for this channel at 55 eV electron impact energy. In the present work, we measured directly the KER distribution of this channel, which is shown in Fig. 4(a). It extends from 2 to 10 eV with a major peak value at 4.8 eV and a slight shoulder around 3.6 eV. Such KER distributions were also obtained by several groups using synchrotron radiation [5,6,28] and highly charged ions [31]. All the works reported a broad range of KER from 2 to 10 eV with a maximum at about 4–5 eV, which is consistent with the present results. Gaire *et al.* [6], in their photo-double-ionization experiments by 42 eV photons, observed two peaks at 4.75 and 3.75 eV in the KER distribution. According to their theoretical calculations of PESs, $^3\Pi_u$ and $^1\Pi_u$ states are apparently dissociative in the C-H coordinate and are most likely responsible for the higher KER peak, while the lower KER structure may stem from the lowest $^3\Sigma_g^-$ electronic state with high enough vibrational excitation to overcome the potential barrier. Gong *et al.* [44] observed a pronounced peak at about 3.7 eV and a weak structure at about 4.9 eV in their KER distribution using an intense laser field. Although the peak positions are in good agreement with those of ours and Gaire *et al.* [6], the branching ratios for these two pathways are quite different. This may be due to the fact that the strong electric field of the laser lowers the barrier of PES of $^3\Sigma_g^-$ electronic state, making the dissociation easier.

C. H_2^+ formation channel $H_2^+ + C_2^+$

As displayed in Fig. 4(b), the total KER for channel $H_2^+ + C_2^+$ exhibits a narrow distribution with a peak at around 4.4 eV. This fragmentation channel was rarely studied in the literature due to its low cross section [21,22]. Recently, Xu *et al.* [20] have reported an investigation on the fragmentation mechanisms of $C_2H_2^{2+}$ into $H_2^+ + C_2^+$ fragment ions induced by 200 keV He^{2+} collisions. With the

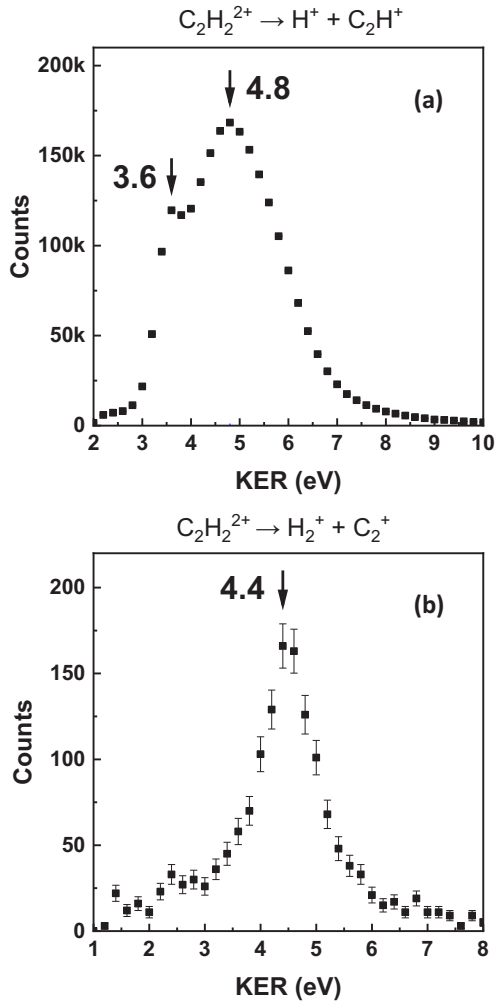

FIG. 4. KER distributions for (a) channel $H^+ + C_2H^+$ and (b) channel $H_2^+ + C_2^+$.

help of quantum chemical calculations, they concluded that $C_2H_2^{2+}$ is first populated to the $^3\Pi$ excited electronic state, followed by acetylene-vinylidene isomerization, and finally the vinylidene-like intermediate dissociates to $H_2^+(^2\Sigma_g^+) + C_2^+(^4\Sigma_g^-)$ [20]. The KER value obtained in the present work is in good agreement with the experimental value (4.45 eV) and the calculated value (4.14 eV) of Xu *et al.* [20], indicating that $C_2H_2^{2+}$ created by 1 keV electron impact might fragment to $H_2^+ + C_2^+$ with the same mechanisms as those of 200 keV He^{2+} collisions.

D. Symmetric breakup channel $CH^+ + CH^+$ and vinylidene decarbonation channel $C^+ + CH_2^+$

Concerning the C-C bond break channels, i.e., $C^+ + CH_2^+$ and $CH^+ + CH^+$ channels, they are not well separated in the TOF correlation map. To disentangle them, we propose an analysis method, which is schematically demonstrated in Fig. 5. The incident electron beam along the x-axis doubly ionizes a molecule at reaction center O, leading to two-body fragmentation, and the two fragment ions fly in opposite directions. We define dissociation angle θ_M as the angle between the momentum of one of the ions (ion1) and the z-axis. In

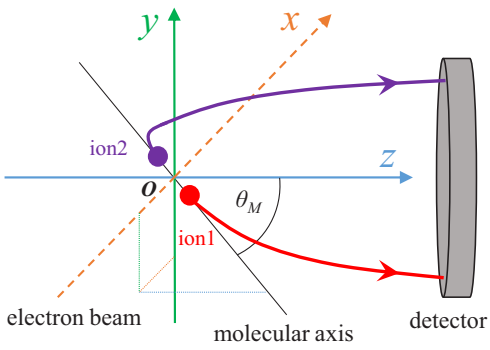

FIG. 5. Schematic for two-body fragmentation of a molecule by electron collision. θ_M is defined as the angle between the momentum of ion1 and the z-axis.

the present experiment, the target molecules are randomly orientated. The axial symmetry of the spectrometer assures that KER for a two-body fragmentation channel is independent of θ_M. Therefore, if we plot 2D density distribution as a function of KER and θ_M, the events for the relevant channel should distribute on a vertical line. As a demonstration, KER-θ_M spectra for $H^+ + C_2H^+$ and $H_2^+ + C_2^+$ channels are plotted in Fig. 6. It is clearly evident that the events for a specific channel distribute around a vertical line, KER = 4.8 eV for $H^+ + C_2H^+$ and KER = 4.4 eV for $H_2^+ + C_2^+$.

However, if the fragmentation channel is falsely identified, the 2D density distribution will be plotted based on incorrect masses of fragment ion pairs. The KER should then vary with angle θ_M. This feature can be used to disentangle channel $CH^+ + CH^+$ and channel $C^+ + CH_2^+$. Figure 7(a) shows a 2D density plot as a function of KER and θ_M by assuming that island c in the inset of Fig. 3 is contributed only from channel $CH^+ + CH^+$. In this plot, two distinct structures can be observed. The major one distributes along the vertical line at KER ~5.0 eV, which is independent of θ_M and can be assigned to the pure true coincidence events from channel $CH^+ + CH^+$, while the events scattering diagonally from 2 to 15 eV should come from the false identification of ion pairs [see the black dashed line in Fig. 7(a)]. To obtain the KER distribution of channel $CH^+ + CH^+$, we choose events within $\theta_M \in [0°, 10°]$, which is completely separated from the background. The obtained KER distribution is displayed in Fig. 7(b), which exhibits a peak value at ~5.0 eV and a pronounced shoulder around 8.0 eV. Such KER spectrum distributions were also obtained experimentally using synchrotron radiation [6,28], highly charged ions [31], as well as an intense laser field [44]. The previous works reported a dominant peak at KER about 5.0 eV. Falcinelli *et al.* [28] observed also a distinct shoulder at about 8.0 eV, while Gong *et al.* [44] reported a sharp peak at ~6.2 eV and a weak broad structure at about 8.0 eV as well. These structures can be assigned to three groups of electronic states for $C_2H_2^{2+}$ based on the calculated PESs along the C-C coordinate by Gaire *et al.* [6]. Dissociation from three low-lying states ($^3\Sigma_g^-$, $^1\Delta_g$, $^1\Sigma_g^+$) with high enough vibrational excitation dominates the lowest peak at 5.0 eV. Three excited states ($^1\Sigma_u^-$, $^3\Sigma_u^+$, $^3\Delta_u$) are apparently dissociative and contribute to the broad structure at around 8.0 eV, while an ~6.0 eV peak may be

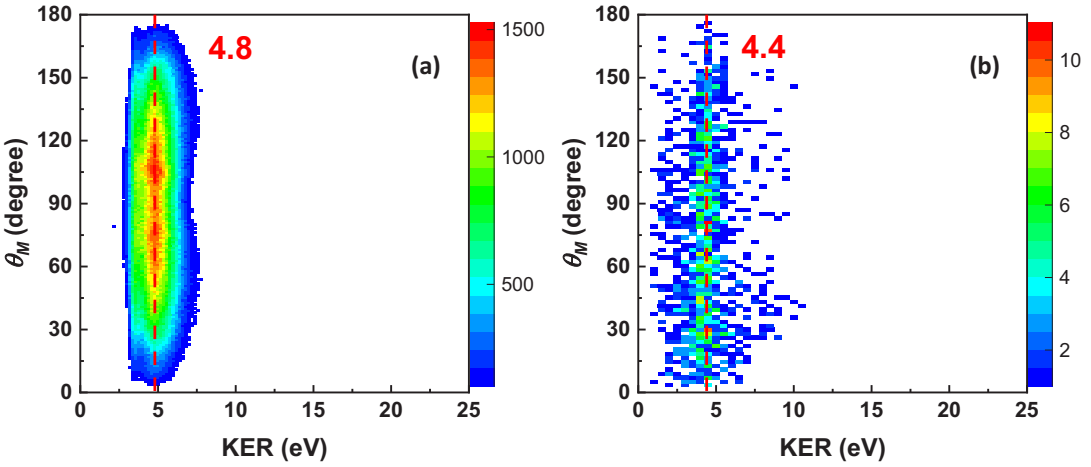

FIG. 6. KER-θ_M spectra for (a) channel $H^+ + C_2H^+$ and (b) channel $H_2^+ + C_2^+$.

contributed from the dissociation from three Π states ($^3\Pi_u$, $^1\Pi_u$, $^3\Pi_g$) possibly through the conical intersection with $^1\Sigma_u^-$, $^3\Sigma_u^+$, and $^3\Delta_u$.

On the other hand, if we assume that island *c* is contributed only from channel $C^+ + CH_2^+$ and plot 2D density once again, the situation will be different. The result is shown in Fig. 8(a). This time, a narrow vertical line along KER ∼4.5 eV can be observed, corresponding to the pure true coincidence events from channel $C^+ + CH_2^+$. In this way, we successfully disentangle the events on island *c* in Fig. 3 which belong to two separate channels. The KER distribution for the events within $\theta_M \in [0°, 10°]$ from channel $C^+ + CH_2^+$ is drawn in Fig. 8(b). A narrow peak at 4.5 eV and a broad structure around 5–7 eV can be identified. Due to the embedded isomerization processes, this fragmentation channel has been intensively investigated both experimentally and theoretically in recent years. Flammini *et al.* [18] reported a total KER value of 5.9 ± 2.7 eV for this channel in their Auger-electron-ion-ion coincidence experiment by electron impact at 4 keV, while King *et al.* [29] determined a single KER of 3.5 ± 0.5 eV following ionization by 65 eV electrons. There are several reported KER distributions measured using synchrotron radiation [5,6,28], an intense laser field [44], and highly charged ion [31]. The previous works reported a KER peak at ∼4.5 eV, consistent with the present result. Zhang *et al.* [31] observed also a broad structure at ∼6.0 eV in their ion collision experiment. Zyubina *et al.* [7] calculated the transition states corresponding to the pathways of isomerization dissociation from two lowest states ($^3\Sigma_g^-$, $^1\Delta_g$) of $C_2H_2^{2+}$. Based on the calculation, these two states can contribute to the observed low KER peak at about 4.5 eV, while Osipov *et al.* [5], who performed a combined experimental and computational study, suggested that two low-lying excited states ($^1\Delta_g$, $^1\Sigma_g^+$) of $C_2H_2^{2+}$ should be responsible for the low KER peak, among which they believed that $^1\Sigma_g^+$ state is dominated. As for the broad structure at ∼6.0 eV, Zhang *et al.* [31] assigned it to the higher excited state of $C_2H_2^{2+}$, namely the $^3\Pi_u$ state. Actually, Zyubina *et al.* [7] calculated the transition states for isomerization dissociation pathways from the $^3\Pi$ state and the relevant KER is estimated to be 6.3 eV, in reasonable agreement with the broad structure around 6.0 eV.

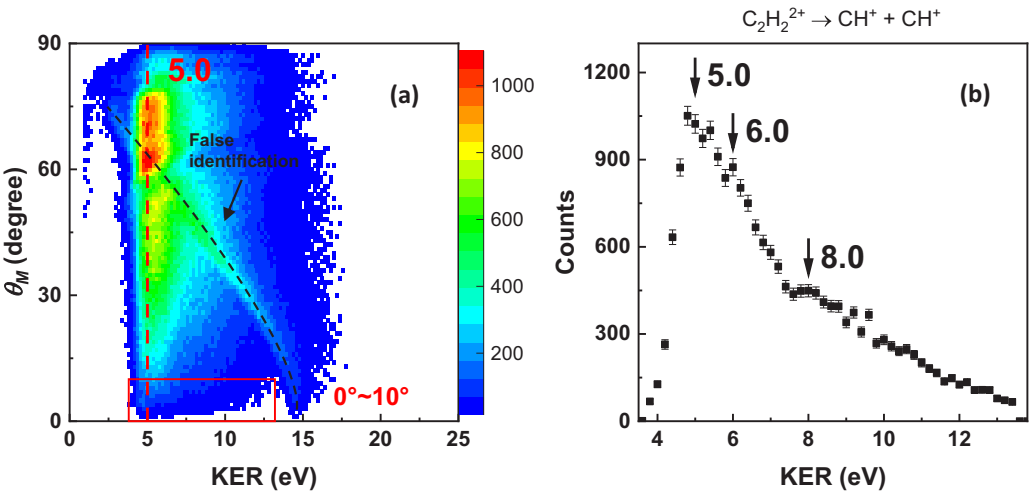

FIG. 7. (a) KER-θ_M spectrum obtained by assuming that only ion pairs CH^+/CH^+ were produced. (b) KER distribution for events selected by the red box in (a).

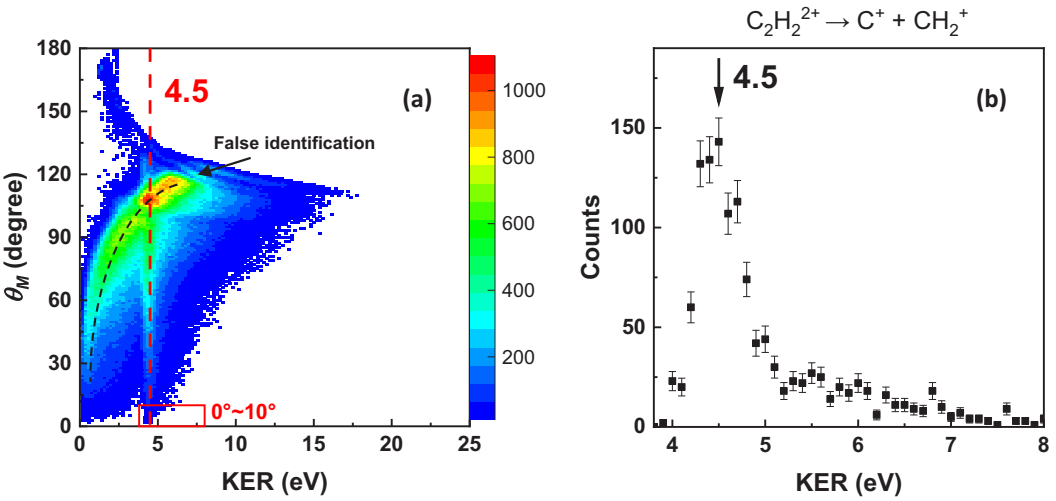

FIG. 8. (a) KER-θ_M spectrum obtained by assuming that only ion pairs C^+/CH_2^+ were produced. (b) KER distribution for events selected by the red box in (a).

E. Branching ratios for two-body fragmentation channels of $C_2H_2^{2+}$

Since all four two-body fragmentation channels have been separated successfully, we are able to determine the relative branching ratios by simply calculating the count ratio of the events within the same angle range $\theta_M \in [0^\circ, 10^\circ]$. The counts for channel $CH^+ + CH^+$ should be multiplied by a factor of $1/2$ since the two identical fragments cannot be distinguished leading to the first hit ion only distributed within an angle range $0^\circ \leqslant \theta_M \leqslant 90^\circ$. Within the same selected angle condition, the event density is doubled compared to that of the full-angle distribution channels. For deprotonation channel $H^+ + C_2H^+$, the long tail in Fig. 3 originating from a long-lived metastable dication should also be taken into account. The percentage of relative branching ratios for these four channels are listed in Table II. The results from some of the previous works are also listed in the table for comparison. Among the four two-body fragmentation channels, the deprotonation channel dominates with a branching ratio of 63.3%, while the branching ratios for $CH^+ + CH^+$ and $C^+ + CH_2^+$ channels are 32.6% and 4.08%, respectively, consistent with the electron impact result of King *et al.* [30] at 200 eV collision energy. The H_2^+ formation channel is observed in present experiment despite the low cross section. The branching ratio is determined to be 0.02%, in good agreement with the result of Saito *et al.* [22] in their photoion-photoion coincidence experiment at 270 eV photon energy.

IV. SUMMARY

To sum up, two-body fragmentation of $C_2H_2^{2+}$ dication is investigated utilizing a newly built ion momentum imaging spectrometer equipped with a photoelectron emission gun. Two fragmentation channels of $C_2H_2^{2+} \rightarrow H^+ + C_2H^+$ and $C_2H_2^{2+} \rightarrow H_2^+ + C_2^+$ can be directly identified from the TOF correlation map, while the other two channels of $C_2H_2^{2+} \rightarrow CH^+ + CH^+$ and $C_2H_2^{2+} \rightarrow C^+ + CH_2^+$ are disentangled by developing an analysis method based on the fact that the KER is independent of the dissociation angle θ_M. The KER distributions and relative abundance of these four channels are obtained.

For the deprotonation channel $H^+ + C_2H^+$, a major peak at 4.8 eV and a shoulder at 3.6 eV are observed in the KER distribution. The analysis indicates that the KER peak at

TABLE II. Relative branching ratios for two-body fragmentation channels of $C_2H_2^{2+}$.

	Branching ratios (%)						
	Electron impacts		Intense laser	Photoionization			Ion impacts
Channel	Present	200 eV[a]	790 nm[b]	42 eV[c]	270 eV[d]	285.8 eV[d]	3 keV/u Ar^{8+} ion[e]
$H^+ + C_2H^+$	63.3	64.4	58	84.1	54.5	53.3	57
$H_2^+ + C_2^+$	0.02				0.03	0.7	
$CH^+ + CH^+$	32.6	33.0	19	12.6	36.6	41.1	40
$C^+ + CH_2^+$	4.08	2.6	23	3.3	8.87	4.9	3

[a]Reference [30].
[b]Reference [44].
[c]Reference [6].
[d]Reference [22].
[e]Reference [31].

4.8 eV could be ascribed to the dissociative electronic states $^3\Pi_u$ and $^1\Pi_u$, while the shoulder at 3.6 eV KER may stem from the lowest $^3\Sigma_g{}^-$ electronic state. The KER spectrum for the $H_2{}^+$ formation channel ($H_2{}^+ + C_2{}^+$) exhibits a narrow distribution with a peak at about 4.4 eV. Xu *et al.* [20] concluded that $C_2H_2{}^{2+}$ is first populated to a $^3\Pi$ electronic state, followed by acetylene-vinylidene isomerization and the vinylidene-like intermediate dissociates to $H_2{}^+(^2\Sigma_g{}^+) + C_2{}^+(^4\Sigma_g{}^-)$. According to their calculations of transition states, a KER value of 4.14 eV was determined, consistent with the measured KER value. The KER distribution for the symmetric breakup channel $CH^+ + CH^+$ shows a peak value at ∼5.0 eV and a pronounced shoulder around 8.0 eV. A slight structure at ∼6.0 eV is also visible. Based on the calculated PESs along the C-C coordinate by Gaire *et al.* [6], these structures can mainly be ascribed to three groups of electronic states for $C_2H_2{}^{2+}$, i.e., three low-lying electronic states ($^3\Sigma_g{}^-$, $^1\Delta_g$, $^1\Sigma_g{}^+$) contribute to the structure at KER about 5.0 eV, and three excited states ($^1\Sigma_u{}^-$, $^3\Sigma_u{}^+$, $^3\Delta_u$) to the 8.0 eV peak, while the peak at ∼6.0 eV can be contributed from the dissociation from the three Π states ($^3\Pi_u$, $^1\Pi_u$, $^3\Pi_g$) possibly through conical intersection with $^1\Sigma_u{}^-$, $^3\Sigma_u{}^+$, and $^3\Delta_u$. As for vinylidene decarbonation channel $C^+ + CH_2{}^+$, a narrow peak at 4.5 eV and a broad structure around 5–7 eV are identified in the KER distribution. Zyubina *et al.* [7] calculated the transition states corresponding to the pathways of isomerization dissociation from electronic states ($^3\Sigma_g{}^-$, $^1\Delta_g$, $^3\Pi$) of $C_2H_2{}^{2+}$. Based on the calculation, the KER values for these three pathways are estimated to be 4.5, 4.0, and 6.3 eV, respectively, which are in reasonable agreement with the experimental data.

ACKNOWLEDGMENT

This work is supported by the National Key Research and Development Program of China (2017YFA0303500) and the National Natural Science Foundation of China (Grants No. 11534011 and No. 11774281).

[1] J. Roithová and D. Schröder, Phys. Chem. Chem. Phys. **9**, 731 (2007).
[2] R. Dörner, V. Mergel, O. Jagutzki, L. Spielberger, J. Ullrich, R. Moshammer, and H. Schmidt-Böcking, Phys. Rep. **330**, 95 (2000).
[3] J. Ullrich, R. Moshammer, A. Dorn, R. Dörner, L. P. H. Schmidt, and H. Schmidt-Böcking, Rep. Prog. Phys. **66**, 1463 (2003).
[4] R. Thissen, J. Delwiche, J. M. Robbe, O. Duflot, J. P. Flament, and J. H. D. Eland, J. Chem. Phys. **99**, 6590 (1993).
[5] T. Osipov, T. N. Rescigno, T. Weber, S. Miyabe, T. Jahnke, A. S. Alnaser, M. P. Hertlein, O. Jagutzki, L. Ph. H. Schmidt, M. Schöffler *et al.*, J. Phys. B **41**, 091001 (2008).
[6] B. Gaire, S. Y. Lee, D. J. Haxton, P. M. Pelz, I. Bocharova, F. P. Sturm, N. Gehrken, M. Honig, M. Pitzer, D. Metz *et al.*, Phys. Rev. A **89**, 013403 (2014).
[7] T. S. Zyubina, Y. A. Dyakov, S. H. Lin, A. D. Bandrauk, and A. M. Mebel, J. Chem. Phys. **123**, 134320 (2005).
[8] A. M. Mebel, T. S. Zyubina, Y. A. Dyakov, A. D. Bandrauk, and S. H. Lin, Int. J. Quantum Chem. **102**, 506 (2005).
[9] D. Duflot, J -M. Robbe, and J -P. Flament, J. Chem. Phys. **102**, 355 (1995).
[10] J. Palaudoux and M. Hochlaf, J. Chem. Phys. **126**, 044302 (2007).
[11] B. Wolter, M. G. Pullen, A.-T. Le, M. Baudisch, K. Doblhoff-Dier, A. Senftleben, M. Hemmer, C. D. Schröter, J. Ullrich, T. Pfeifer *et al.*, Science **354**, 308 (2016).
[12] H. Ibrahim, B. Wales, S. Beaulieu, B. E. Schmidt, N. Thiré, E. P. Fowe, É. Bisson, C. T. Hebeisen, V. Wanie, M. Giguére *et al.*, Nat. Commun. **5**, 4422 (2014).
[13] Z. Li, L. Inhester, C. Liekhus-Schmaltz, B. F. E. Curchod, J. W. Snyder Jr., N. Medvedev, J. Cryan, T. Osipov, S. Pabst, O. Vendrell *et al.*, Nat. Commun. **8**, 453 (2017).
[14] C. E. Liekhus-Schmaltz, I. Tenney, T. Osipov, A. Sanchez-Gonzalez, N. Berrah, R. Boll, C. Bomme, C. Bostedt, J. D. Bozek, S. Carron *et al.*, Nat. Commun. **6**, 8199 (2015).
[15] E. Wells, C. E. Rallis, M. Zohrabi, R. Siemering, B. Jochim, P. R. Andrews, U. Ablikim, B. Gaire, S. De, K. D. Carnes *et al.*, Nat. Commun. **4**, 2895 (2013).
[16] T. Osipov, C. L. Cocke, M. H. Prior, A. Landers, T. Weber, O. Jagutzki, L. Schmidt, H. Schmidt-Böcking, and R. Dörner, Phys. Rev. Lett. **90**, 233002 (2003).
[17] A. S. Alnaser, I. Litvinyuk, T. Osipov, B. Ulrich, A. Landers, E. Wells, C. M. Maharjan, P. Ranitovic, I. Bocharevа, D. Ray *et al.*, J. Phys. B **39**, S485 (2006).
[18] R. Flammini, E. Fainelli, F. Maracci, and L. Avaldi, Phys. Rev. A **77**, 044701 (2008).
[19] A. Hishikawa, A. Matsuda, M. Fushitani, and E. J. Takahashi, Phys. Rev. Lett. **99**, 258302 (2007).
[20] S. Xu, H. Zhao, X. Zhu, D. Guo, W. Feng, K.-C. Lau, and X. Ma, Phys. Chem. Chem. Phys. **20**, 27725 (2018).
[21] J. Laksman, D. Célin, M. Gisselbrecht, S. E. Canton, and S. L. Sorensen, J. Chem. Phys. **131**, 244305 (2009).
[22] N. Saito, M. Nagoshi, M. Machida, I. Koyano, A. De Fanis, and K. Ueda, Chem. Phys. Lett. **393**, 295 (2004).
[23] Y. H. Jiang, A. Rudenko, O. Herrwerth, L. Foucar, M. Kurka, K. U. Kühnel, M. Lezius, M. F. Kling, J. van Tilborg, A. Belkacem *et al.*, Phys. Rev. Lett. **105**, 263002 (2010).
[24] X. Gong, Q. Song, Q. Ji, K. Lin, H. Pan, J. Ding, H. Zeng, and J. Wu, Phys. Rev. Lett. **114**, 163001 (2015).
[25] M. E.-A. Madjet, O. Vendrell, and R. Santra, Phys. Rev. Lett. **107**, 263002 (2011).
[26] D. Luo, B. Wei, Y. Zhang, Y. Zou, R. Hutton, F. Chen, and X. Wang, J. Phys. B **51**, 165203 (2018).
[27] S. De, J. Rajput, A. Roy, P. N. Ghosh, and C. P. Safvan, Phys. Rev. A **77**, 022708 (2008).
[28] S. Falcinelli, M. Alagia, J. M. Farrar, K. S. Kalogerakis, F. Pirani, R. Richter, L. Schio, S. Stranges, M. Rosi, and F. Vecchiocattivi, J. Chem. Phys. **145**, 114308 (2016).
[29] M. Alagia, C. Callegari, P. Candori, S. Falcinelli, F. Pirani, R. Richter, S. Stranges, and F. Vecchiocattivi, J. Chem. Phys. **136**, 204302 (2012).
[30] S. J. King and S. D. Price, J. Chem. Phys. **127**, 174307 (2007).

[31] Y. Zhang, B. Wang, L. Wei, T. Jiang, W. Yu, R. Hutton, Y. Zou, L. Chen, and B. Wei, J. Chem. Phys. **150**, 204303 (2019).
[32] Y. H. Jiang, A. Senftleben, M. Kurka, A. Rudenko, L. Foucar, O. Herrwerth, M. F. Kling, M. Lezius, J. V. Tilborg, A. Belkacem, R. Moshammer *et al.*, J. Phys. B **46**, 164027 (2013).
[33] A. Matsuda, M. Fushitani, R. D. Thomas, V. Zhaunerchyk, and A. Hishikawa, J. Phys. Chem. A **113**, 2254 (2009).
[34] A. C. O. Guerra, J. B. Maciel, C. C. Turci, H. Ikeura-Sekiguchi, and A. P. Hitchcock, Chem. Phys. **326**, 589 (2006).
[35] M. S. Arruda, A. Medina, J. N. Sousa, L. A. V. Mendes, R. R. T. Marinho, and F. V. Prudente, J. Phys. Chem. A **120**, 5325 (2016).
[36] A. Matsuda, M. Fushitani, E. J. Takahashi, and A. Hishikawa, Phys. Chem. Chem. Phys. **13**, 8697 (2011).
[37] R. Flammini, M. Satta, E. Fainelli, and L. Avaldi, Phys. Chem. Chem. Phys. **13**, 19607 (2011).
[38] X. Ren, T. Pflüger, M. Weyland, W. Y. Baek, H. Rabus, J. Ullrich, and A. Dorn, J. Chem. Phys. **141**, 134314 (2014).
[39] W. C. Wiley and I. H. McLaren, Rev. Sci. Instrum. **26**, 1150 (1955).
[40] S. E. Sobottka and M. B. Williams, IEEE Trans. Nucl. Sci. **35**, 348 (1988).
[41] O. Jagutzki, V. Mergel, K. Ullmann-Pfleger, L. Spielberger, U. Spillmann, R. Dörner, and H. Schmidt-Böcking, Nucl. Instrum. Methods Phys. Res. A **477**, 244 (2002).
[42] E. Wang, Y. Tang, Z. Shen, M. Gong, X. Shan, and X. Chen, Rev. Sci. Instrum. **86**, 066108 (2015).
[43] S. Larimian, S. Erattupuzha, E. Lötstedt, T. Szidarovszky, R. Maurer, S. Roither, M. Schöffler, D. Kartashov, A. Baltuška, K. Yamanouchi *et al.*, Phys. Rev. A **93**, 053405 (2016).
[44] X. Gong, Q. Song, Q. Ji, H. Pan, J. Ding, J. Wu, and H. Zeng, Phys. Rev. Lett. **112**, 243001 (2014).